Feasibility of multi-centric fMRI connectivity studies of Alzheimer's disease

Christian Dansereau[a,b], Celine Risterucci[c], Emilio Merlo Pich[c], Douglas Arnold[d], Pierre Bellec[a,b,*]

[a] *Centre de Recherche de l'Institut Universitaire de Gériatrie de Montréal, Montréal, CA*
[b] *Département d'Informatique et de recherche opérationnelle, Université de Montréal, Montréal,CA*
[c] *F. Hoffmann-La Roche Ldt., Basel, Switzerland*
[d] *NeuroRx, Montreal, Quebec, Canada*

Abstract

Keywords: fmri, effect size, multisite, clinical trial, AD biomarker

Highlights

- etc

1. Introduction

Resting-state (RS) connectivity in fMRI is a promising biomarker for a variety of neurological diseases. Typically, in a clinical trial, a large cohort is recruited and evaluated at multiple sites spread over countries or even continents. In academia the budget allowed per investigator for scanning is generally of the order of 30 to 50 subjects leading two small cohorts, one problem with small sample size is the difficulty to detect small and consistent effect (differences) between groups. A solution that can help on this from is to increase the number of subject by pooling small RS cohorts acquired on the same scanner or on different scanners, this approach is referred to has multi-site . The main potential issue with that approach is the lack of consistency in the multi-site RS connectivity acquisitions that may obscure clinically relevant information. Therefore the aims of the study were to: (1) characterize the amplitude of the site bias, i.e. the systematic differences in rs-fMRI connectivity across different acquisition sites; (2) Quantify the impact of the between-site variance on the power of statistical tests in resting-state fMRI.

In most experiments conducted in neuroimaging, the main factors that influence power are: (1) the size of the effect, determined by the difference of the

*Corresponding author
Email address: pierre.bellec@criugm.qc.ca (Pierre Bellec)

mean connectivity of one group versus a control group and the variability of this difference across subjects and groups; and (2) the sample size, i.e. the number of subjects in the study (Desmond and Glover, 2002). This last factor is usually the only one controlled by the investigator, hence why an increasing number of researchers share multicentric, sometimes multiprotocol, data suitable to statistical analysis. In research it is very difficult to obtain a grant large enough to scan a cohort larger than 80 subjects, therefore researcher and consortium initiatives have started to pool their resources together to make initiative composed of publicly available large cohorts of subjects like the 1000 functional connectome (Biswal et al., 2010), ADNI (Mueller et al., 2005), among others. In clinical trial the justification for multicentric acquisition is more of a logistical one then a financial reason; they need to recruit a large amount of subject in a short period of time. In order to achieve this goal they mandate the recruitment to multiple clinical centers across the globe which accelerate the evaluation time of a drug. Although these centers may be similar by their scanner protocols, scanners will have difference in their software version, specific add-on to the scanners, and, most importantly, vendors (even field strength may differ in some cases). Unfortunately between studies, MR acquisition methodologies are among the most commonly cited sources of measurement variation (Friedman et al., 2006). This is why it is important to assess if multi-site resting-state connectivity analysis are feasible (we can combine the data from multiple sources while introducing a reasonable amount of variance which is still acceptable to detect effects in the data) and what corrective measure on the data should be applied to reduce the bias introduced by multi-site analysis. Among the factor of variability across sites, we can list the following 3 categories described in (Yan et al., 2013b):

Difficulty of increasing the sample size

- Collecting a large sample size is very expensive.
- Recruitment may be difficult at a single site.
- Large sample size can be achieved in multisite study.
- Multisite studies come with problems of their own.

Source of variance across sites.

- **Inclusion/exclusion criteria.**
- **Socio-cultural characteristics of recruiting sites**
  (e.g., ethnicity, language, diet, socioeconomic status).
- **Acquisition-related factors**
  (e.g., scanner make and model, sequence type, coil type, repetition time, flip angle, acquisition volume, etc).
- **Experimental design-related variations**
  (e.g., eyes-open/closed, experiment duration, instruction to participant).

- **Environmental-related variations**
  (e.g., sound, room temperature, head-motion restraint).

1. *Acquisition-related variations:*
   (a) *Scanner make and model (Friedman et al., 2006)*
   (b) *Sequence type (spiral vs. echo planar; single-echo vs. multi-echo) (Klarhofer et al., 2002), parallel vs. conventional acquisition (Feinberg et al., 2010) (Lin et al., 2005)*
   (c) *Coil type (surface vs. volume, number of channels, orientation).*
   (d) *Acquisition parameters: repetition time, number of repetitions, flip angle, echo time, and acquisition volume (field of view, voxel size, slice thickness/gaps, slice prescription) (Friedman and Glover, 2006).*
2. *Experimental-related variations:*
   (a) *Participant instructions (Hartstra et al., 2011), eyes-open/eyes-closed (Yan et al., 2009) (Yang et al., 2007), visual displays, experiment duration (Fang et al., 2007) (Van Dijk et al., 2010).*
3. *Environment-related variations:*
   (a) *Sound attenuation measures (Cho et al., 1998) (Elliott et al., 1999).*
   (b) *Attempts to improve participant comfort during scans (e.g., music, videos) (Cullen et al., 2009).*
   (c) *Head-motion restraint techniques (e.g., vacuum pad, foam pad, bite-bar, plaster cast head holder) (Edward et al., 2000) (Menon et al., 1997).*
   (d) *Room temperature and moisture (Vanhoutte et al., 2006).*

In 2009, the publicly released 1000 Functional Connectomes Project (FCP) and International Neuroimaging Data-sharing Initiative (INDI) provided a glimpse of the variability in imaging methodologies employed by the neuroimaging field. The dataset includes rs-fMRI samples independently collected at imaging sites around the world. A noteworthy aspect of this dataset is the variation in almost every parameter of the imaging acquisition methodologies, while the majority of subject-related variables are not reported (due in most cases, to the fact that they were not thoroughly recorded). Despite justifiable scepticism, feasibility analyses demonstrated that meaningful explorations of the aggregate dataset, composed of 24 imaging sites for a grand total of 1093 subjects, could be performed (Biswal et al., 2010). Although no explicit correction for multi-site variability was used, they only use global signal correction (GSC) to normalize subjects which may introduce anti-correlation in the data (Fox et al., 2009; Murphy et al., 2009; Saad et al., 2012; Carbonell et al., 2014; Power et al., 2014). After accounting for site-related differences, the analysis showed brain-behaviour relationships with phenotypic variables such as age, gender, and diagnostic label, and confirmed a variety of prior hypotheses (Biswal et al., 2010; Fair et al., 2012; Tomasi and Volkow, 2010; Zuo et al., 2012). While encouraging, many uncontrolled and unknown factors in the 1000 FCP remain a source of concern, as they spread beyond simple site effects and can limit the datasets utility as

highlighted by Yan et al. (2013a). An other compelling proof of multi-site bias is the study reported by Nielsen et al. (2013) where they did an analysis on a single site dataset and a multi-site dataset of subject with autism and concluded that the multi-site autism study classification accuracy significantly outperformed chance but was much lower for multi-site prediction than for previous single site results (Nielsen et al., 2013). We therefore need to keep in mind that the site effect must be taken in account in the analysis or we may reduce our detection power.

Specific objectives.

- Propose a method to account for multisite variance in a general linear model analysis.
- Amount of variance intra-site and inter-site.
- Quantify the impact of inter-site biases on the detection power of a rs-fMRI effect.
  - How sample size in multi-centric topology impact sensitivity.
  - How group balancing in multi-centric topology impact sensitivity.
  - Interaction of site-pathology and it's impact on detection power.

Other info. Cite for the urgency of using pool mutisite data for neuro-imaging analysis Cheng et al. (2015).

2. Method

2.1. Data samples

Participants. The paper studies 345 cognitively normal young adults (CNY) from the 1000 functional connectome project[1] (150 males, age range = 18-46 yrs) as a reference dataset. One of the particularity of this dataset is the presence of one large site of ~ 200 subjects and 7 small sites of ~ 20 subjects per site. We are therefore able to simulate realistic scenarios where we model the variability of a real monosite and the variability introduce by combining small sites into a large sample of the same total sample size, see Table 1 for more details on each site. The experimental protocols for all datasets were approved by there respective ethic boards.

Acquisition. We need to discuss how to present this data (I dont have the details for each site...)

[1] `http://fcon_1000.projects.nitrc.org/`

2.2. Preprocessing

The datasets were analysed using the NeuroImaging Analysis Kit (NIAK[2]) version 0.12.14, under CentOS version 6.3 with Octave[3] version 3.8.1 and the Minc toolkit[4] version 0.3.18. Analyses were executed in parallel on the "Mammouth" supercomputer[5], using the pipeline system for Octave and Matlab (Bellec et al., 2010a), version 1.0.2. Brain map visualizations were created using MRICron software Rorden et al. (2007). Each fMRI dataset was corrected of inter-slice difference in acquisition time and the parameters of a rigid-body motion was estimated for each time frame. Rigid-body motion was estimated within as well as between runs, using the median volume of the first run as a target. The median volume of one selected fMRI run for each subject was coregistered with a T1 individual scan using Minctracc (Collins et al., 1998), which was itself non-linearly transformed to the Montreal Neurological Institute (MNI) template (Fonov et al., 2011) using the CIVET pipeline (Zijdenbos et al., 2002). The MNI symmetric template was generated from the ICBM152 sample of 152 young adults, after 40 iterations of non-linear coregistration. The rigid-body transform, fMRI-to-T1 transform and T1-to-stereotaxic transform were all combined, and the functional volumes were resampled in the MNI space at a 3 mm isotropic resolution. A censoring method described in (Power et al., 2012) called "scrubbing" was used to remove the volumes with excessive motion using a cut-off value of $FD \geq 0.5$. A minimum number of 50 unscrubbed volumes per run, corresponding to ~ 125 s of acquisition for a TR of 2.5 seconds, was then required for further analysis. The following nuisance parameters were regressed out from the time series at each voxel: slow time drifts (basis of discrete cosines with a 0.01 Hz high-pass cut-off), average signals in conservative masks of the white matter and the lateral ventricles as well as the first principal components (95% energy) of the six rigid-body motion parameters and their squares (Lund et al., 2006),(Giove et al., 2009). The fMRI volumes were finally spatially smoothed with a 6 mm isotropic Gaussian blurring kernel.

2.3. Functional networks

Functional parcellation. Regions are routinely defined using an anatomical parcellation (He et al., 2009), such as the AAL template (Tzourio-Mazoyer et al., 2002). Anatomical parcels may however not well match the brain functional organization. In this work, we used functional brain parcellations, aimed at defining groups of brain regions with homogeneous time series. A number of algorithms have been proposed with additional spatial constraints, to ensure that the resulting parcels are spatially connected (Lu et al., 2003; Thirion et al., 2006; **?**). We can achieve this aim and reduce the computational burden of the

[2] `http://www.nitrc.org/projects/niak/`

[3] `http://gnu.octave.org`

[4] `http://www.bic.mni.mcgill.ca/ServicesSoftware/ServicesSoftwareMincToolKit`

[5] `http://www.calculquebec.ca/index.php/en/resources/compute-servers/mammouth-parallele-ii`

analysis using a region-growing algorithm Bellec (2006), resulting in more homogeneous regions composed of temporally similar and contiguous voxels. The spatial dimension was selected arbitrarily by setting the size where the growing process stopped (a threshold of 1000 mm3 resulted into R=957 regions) from a reference dataset of healthy adults from the 1000 functional connectome project (Cambridge cohort (Biswal et al., 2010), parcellation available here 4b). The regions were built to maximize the homogeneity of the time series within the region, i.e. the average correlation between the time series associated with any pair of voxels of the region. The region growing was applied on the time series concatenated across all subjects (after correction to zero mean and unit variance), such that the homogeneity was maximized on average for all subjects, and the small homogeneous regions are identical for all subjects. Because of the temporal concatenation of time series, we had to limit the memory demand, and the region-growing was thus applied independently in each of the 116 areas of the AAL template (Tzourio-Mazoyer et al., 2002). See Bellec (2006) for more details regarding the implementation of the region-growing algorithm. Overall, this process reduced the dataset of each subject into a (T x R) data array, where T is the number of time samples and R is the number of regions.

Functional network decomposition. From a pure functional viewpoint, the spatial constraint seems somewhat arbitrary, as functional units in the brain at low resolution encompass distributed networks of brain regions with homotopic regions often being part of a single parcel (De Luca et al., 2006; Damoiseaux et al., 2006). Some works have thus used distributed parcels as the spatial units to measure functional brain connectivity, e.g. (Jafri et al., 2007; Marrelec et al., 2008). We relied on a recent method called Bootstrap Analysis of Stable Clusters (BASC), which can identify consistent functional networks for a group of subjects (Biswal et al., 2010). using a hierarchical cluster with Wards criterion both at the individual and the group levels. The functional networks can be generated at any arbitrary scale (within the range of the fMRI resolution), and we considered only networks generated at the group level, which were non-overlapping and not necessarily spatially contiguous. In the present work we generated a BASC decomposition in 100 networks.

TODO: cite the NATURE paper of Pierre Orban for parcelation and connections selection.

Functional connectome. Using a brain partition of R networks obtain from BASC procedure described in Bellec et al. (2010b), and taking each pair of distinct networks i and j, the between-network connectivity $y_{i,j}$ is measured by the Fisher transform of the Pearson's correlation between the average time series of the network. The within-network connectivity $y_{i,i}$ is the Fisher transform of the average correlation between time series of every pair of distinct voxels inside network i. The connectome $\mathbf{Y} = (y_{i,j})_{i,j=1}^{R}$ is thus a $R \times R$ matrix. Each column j (or row, as the matrix is symmetric) codes for the connectivity between network j and all other brain networks (full brain functional connectivity map).

For a scale with R parcels, there are exactly $L = R(R+1)/2$ distinct elements in an individual connectome $\mathbf{Y}$.

2.4. Simulations

Power analysis for a resting-state fMRI study. A Monte-Carlo simulation was implemented to evaluate the power of a resting-state multi-site study. For each site and each sample, $B\%$ of the subjects were randomly assigned to a 'treatment' group. For the subjects in this group, a value was added to achieve a given relative effect size (Cohen's d, i.e. the mean of the two groups divided by the standard deviation of all sites). The significance of the difference between the control and 'treatment' group was assessed by a t-test in a linear model. To account for site-specific bias we have included dummy variables in the GLM model. The study was repeated for various effect sizes (0 to 1.5 with a step of 0.01) at a threshold of 0.001 on the p-value in the t-test.

In order to simulate various scenarios within the context of a multi-site setting, a cohort of subjects acquired at a single-site was selected to act as our reference dataset and for the multi-site configuration a cohort from a collection of small sites, roughly totalling the same sample size as the reference dataset, was used. The simulation was based on a scenario with 8 sites for a total of 345 subjects, and no homogenization of acquisition protocol whatsoever. The multi-site (with correction) is based on 150 subjects from 7 sites and the monosite is based on one site of 195 subjects.

Estimation of the detection sensitivity. Based on the literature review previously described in (TODO: cite the NATURE paper of Orban2015) reporting 10 reproducible pair of regions reported to be affected by Alzheimer disease progression and displayed connectivity changes between cognitively normal subjects and patient with dementia of the Alzheimer type. The following confounding variables were modelled in the general linear model (GLM) analysis: frame displacement (FD). Significance of the results is obtain with a Student t-test and the sensitivity of the test is evaluated by sub-sampling 70% of the dataset ($B = 10^3$ random samples). For each sample b, we have a p-value p_b^* and the detection sensitivity is estimated by the probability of p_b^* being inferior to 0.001.

$$\frac{1}{B}\sum_{b=1}^{B}\left(p_b^* \leq 0.001\right). \tag{1}$$

Effect size (cohen's d). For each site and each sample, half of the subjects were randomly assigned to a "treatment" group and a Monte-Carlo simulation was used to estimate the detection power in the single-site and in multi-site setting.

The normalized Cohen's d was used to estimate the effect size and it is defined as the difference between two means $\bar{x_1}, \bar{x_2}$ divided by a standard deviation from the data s.

For each site an effect is added to the connectivity of $B\%$ of the subjects, selected randomly ("pathological" group):

$$y_{i,j} = y_{i,j} + \mu. \tag{2}$$

The parameter μ is chosen to obtain a particular effect size (measured by the Cohen d)

$$d = \frac{\mu}{s_{i,j}}, \tag{3}$$

where $s_{i,j}$ is the standard deviation between region i and j for the reference population (mono-site, Cambridge). The significance of the difference between the control and 'treatment' group was assessed by a t-test in a linear model, including a covariate to model the motion. The study was repeated for various effect sizes (0 to 0.8 with a step of 0.01) with a p-value threshold of 0.001 on the t-test.

In order to introduce the same effect-size across the single-site and multi-site dataset we are taking the standard deviation from the single-site cohort as the reference. The connection $y_{i,j}$ of the randomly affected subjects ("treatment" group) are therefore calculated $y_{i,j} = y_{i,j} + d \times s_{i,j}$.

multi-site correction approach. In order to obtain an unbiased method to combine sites and do group analysis on them we are using dummy variables (binary vectors $1 \times S$) who code for each site in the GLM model illustrated in Equation4. The variables are corrected to have a zero mean across subjects, and an intercept (i.e. a column filled with 1) is added to $\mathbf{X}$. The GLM relies on the following stochastic model:

$$\mathbf{Y} = \mathbf{X}\beta + \mathbf{V}\gamma + \mathbf{E}, \tag{4}$$

- $\mathbf{Y}$: $N \times 1$, connectivity value for the pair (i, j),
- $\mathbf{X}$: $N \times K$, explainable variables,
- β: $1 \times K$, regression values for each explainable variable,
- $\mathbf{V}$: $N \times S$, each column code for a site (0/1),
- γ: $1 \times S$, site average connectivity,
- $\mathbf{E}$: $N \times 1$, residual values from the regression,

with N the number of subjects, K the number of explainable variables and S the number of sites. Where β is an unknown $1 \times K$ vector of linear regression coefficients, γ is a $1 \times S$ vector of linear regression coefficients representing the contribution of each site and $\mathbf{E}$ is a $N \times 1$ random (noise) multivariate Gaussian variable. As data generated from different subjects are statistically independent, and under an homoscedasticity assumption, the regression coefficients β can be estimated with ordinary least squares. To apply the correction $S - 1$ dummy-variables are added to the model in Equation4 with S being the total number of sites used in the study.

Framewise displacement (FD). Index measure of head motion from one frame to the other. It is calculated as the sum of the absolute values of the differentiated realignment estimates at every time point (Power et al., 2012) this measure give us an approximation of the motion frame by frame in millimeter. We are using this measure as an index of motion estimation.

$$FD_i = |\triangle d_x(t)| + |\triangle d_y(t)| + |\triangle d_z(t)| + |\triangle r_x(t)| + |\triangle r_y(t)| + |\triangle r_z(t)|, \quad (5)$$

$$r_x(t) = 50 \left(\frac{2\pi\alpha_x(t)}{360} \right), \quad (6)$$

with

- $(d_x(t), d_y(t), d_z(t))$ translation parameters (mm),
- $(\alpha_x(t), \alpha_y(t), \alpha_z(t))$ rotation parameters (degres),
- $\triangle$ difference between time t et $t-1$.

3. Results

The first assessment perform on the dataset was to verify the distribution of the variance in functional connectivity among each site and across sites in order to see if they are of the same order of magnitude or not. This analysis of Figure 1 shows the distribution of the standard deviation of connectivity across subjects (the distribution is over the full brain connectome, with several 1000s connections) at the 8 sites against the inter-sites standard deviation of connectomes (average at each site). as we can see the inter-site (between site) variability is smaller than the intra-site (between subjects) variability. As we can see the amplitude of inter-site bias is about 3-fold smaller than the within-site standard deviation (red ˜0.06 vs. orange ˜0.18).

In order to verify how spatial structure vary across sites the average standard deviation and the average connectivity map of the DMN were extracted for each site and reported in Figure 2. As we can see in the intersection between two sites the difference in average connectivity between-sites is illustrated (red set of brain cuts). First the mean DMN at each site is consistent with the expected spatial distribution reported in other studies (Damoiseaux et al., 2006; Dansereau et al., 2014; Yan et al., 2013b). The most salient changes between-sites are located in the mesio-frontal region associated with the anterior part of the DMN. In order to verify if significant changes are not only found in the DMN we have look at the other connectivity patterns and the findings can be generalized to the full connectome see Figure 3.

We also showed using Monte-Carlo simulations that the power of detecting an effect is marginally affected by the site acquisition configuration (single site or multi-site, see Figure) where the sites are balanced in term of the amount of subject with and without the effect.

Figure **??** show the pair of regions used in (TODO ORBAN2015) as candidate marker for functional connectivity changes in Alzheimer disease based on a literature review. We will use the correlation between those regions to estimate the variability across subject and induce some effect in our simulations.

In Figure **??** we show the effect of the sample size on the detection power. As expected we are able to detect smaller and smaller effect size as we increase the sample size. For an effect size of 1 which is considered a large effect we are able to detect significant changes in only 20% of the cases at 40 subjects, 80% at 80 subjects and almost 95% at 120% subjects.

Figure **??** show the effect of debalancing the two groups at various ratio (50%-50% , 30%-70% and 15%-85%) for a total sample size of 120 subjects. Has the debalancing increase our ability to detect effect is diminished. As an example for an effect size of 1 we would detect the effect in 95% of the cases in a 50 balanced scenario, this would go down to 90% in a 30%-70% scenario and to 60% in a 15%-85% debalancing.

Figure **??** show the effect of debalancing the two groups at various ratio (50%-50% , 30%-70% and 15%-85%) with an interaction site-pathology for a total sample size of 120 subjects. Has the debalancing increase our ability to detect effect is diminished. As an example for an effect size of 1 we would detect the effect in 98% of the cases in a 50 balanced scenario, this would go down to 95% in a 30%-70% scenario and to 75% in a 15%-85% debalancing. The particularity of this experiment is the fact that the multisite configuration perform better then the single site meanning that it is better to have interaction of various amplitude across small sites than an average interaction on one large site.

Figure **??** show a scenario of two site one large (80 subjects) and one small ($\sim$ 20 subjects) unbalanced at 30%-70% and the inverse. As we can see the multisite configuration is as good as the monosite.

In order to obtain more control on each of the parameter of the simulation and see if we are able to reproduce previous findings we have used a synthetic model using only synthetic data and the average standard deviation of the Cambridge site connectivity. All plots show four scenarios: The top left plot represent the two configurations one monosite and two sites with correction for multisite differences using dummy variables without site effect. Has expected there is no difference between using 1 large site than combining two site of half the size. The plot on the upper right corner represent the detection power when we apply a site effect on balanced sites, here again not much differences an additive effect is fully compensated by the dummy variables corrective method. the lower left plot represent no site effect but an interaction between site and pathology. An the last plot on the lower right corner show the detection power with a site effect of 0.5 and a interation site pathology.

Figure **??** show the same configuration but the sample size are inverted. Has we can see we have the same pattern as in the real data with...

Figure **??** show a more realistic case in clinical trials where the number of scanning sites is very large and the number of subjects per site is small. There is usually no control on the exact balancing of those sites therefore we

have randomly assign debalancing for each site (between 10% and 90%) and have randomly assigned a number of subject to each site (between 2 and 15 subjects).

4. Discussion

Connectivity bias that can impact interpretation.

Type of scanner most of them are Siemens we may have more variability if combining various brand

Talk about the impact in small acquisition 40 subjects total and the importance of pooling data among PI.

Talk about the impact in clinical trial and best practice.

5. Conclusion

6. Table Legend

Site	Magnet	Scaner brand	Channels	N	N final	Sex	Age	TR	# Slices	# Frames
Baltimore, USA	3T	N/A	N/A	23	21	8M/15F	20-40	2.5	47	123
Berlin, Germany	3T	Siemens Tim Trio	12	26	26	13M/13F	23-44	2.3	34	195
Cambridge, USA	3T	Siemens Tim Trio	12	198	195	75M/123F	18-30	3	47	119
Newark, USA	3T	N/A	N/A	19	17	9M/10F	21-39	2	32	135
NewYork_b, USA	3T	Siemens	N/A	20	18	8M/12F	18-46	2	33	175
Oxford, UK	3T	Siemens Tim Trio	12	22	20	12M/10F	20-35	2	34	175
Queensland, Australia	4T	Bruker	1	19	17	11M/8F	20-34	2.1	36	190
SaintLouis, USA	3T	Siemens Tim Trio	12	31	31	14M/17F	21-29	2.5	32	127

Table 1: 1000 funcitonal connectome dataset

7. Acknowledgments

Parts of this work were presented at the 2013 annual meetings of the organization for human brain mapping (Dansereau et al., 2013), as well as the Alzheimer's Association International Conference (AAIC) (2013) (Boston) (**?**). The authors are grateful to the members of the 1000 functional connectome consortium for publicly releasing there dataset. The computational resources used to perform the data analysis were provided by ComputeCanada[6] and CLUMEQ[7], which is funded in part by NSERC (MRS), FQRNT, and McGill University. This project was funded by NSERC grant number RN000028, a salary award from "Fonds de recherche du Québec – Santé" to PB as well as a salary award by the Canadian Institute of Health Research to CD.

[6] `https://computecanada.org/`
[7] `http://www.clumeq.mcgill.ca/`

References

Bellec, P., Feb. 2006. Longitudinal study of large-scale networks in the human brain using fMRI : Methods and application to motor skill learning. Ph.D. thesis, Université Paris XI, Orsay, Paris.
URL http://exocet.imed.jussieu.fr/~{}pbellec/data/these_bellec.pdf

Bellec, P., Carbonell, F., Perlbarg, V., Evans, A. C., 2010a. A neuroimaging analysis kit for Octave and Matlab.
URL http://code.google.com/p/niak/

Bellec, P., Rosa-Neto, P., Lyttelton, O. C., Benali, H., Evans, A. C., Jul. 2010b. Multi-level bootstrap analysis of stable clusters in resting-state fMRI. NeuroImage 51 (3), 1126–1139.
URL http://dx.doi.org/10.1016/j.neuroimage.2010.02.082

Biswal, B. B., Mennes, M., Zuo, X.-N. N., Gohel, S., Kelly, C., Smith, S. M., Beckmann, C. F., Adelstein, J. S., Buckner, R. L., Colcombe, S., Dogonowski, A.-M. M., Ernst, M., Fair, D., Hampson, M., Hoptman, M. J., Hyde, J. S., Kiviniemi, V. J., Kötter, R., Li, S.-J. J., Lin, C.-P. P., Lowe, M. J., Mackay, C., Madden, D. J., Madsen, K. H., Margulies, D. S., Mayberg, H. S., McMahon, K., Monk, C. S., Mostofsky, S. H., Nagel, B. J., Pekar, J. J., Peltier, S. J., Petersen, S. E., Riedl, V., Rombouts, S. A., Rypma, B., Schlaggar, B. L., Schmidt, S., Seidler, R. D., Siegle, G. J., Sorg, C., Teng, G.-J. J., Veijola, J., Villringer, A., Walter, M., Wang, L., Weng, X.-C. C., Whitfield-Gabrieli, S., Williamson, P., Windischberger, C., Zang, Y.-F. F., Zhang, H.-Y. Y., Castellanos, F. X., Milham, M. P., Mar. 2010. Toward discovery science of human brain function. Proceedings of the National Academy of Sciences of the United States of America 107 (10), 4734–4739.
URL http://dx.doi.org/10.1073/pnas.0911855107

Carbonell, F., Bellec, P., Shmuel, A., Feb 2014. Quantification of the impact of a confounding variable on functional connectivity confirms anti-correlated networks in the resting-state. Neuroimage 86, 343–353.
URL http://dx.doi.org/10.1016/j.neuroimage.2013.10.013

Cheng, W., Palaniyappan, L., Li, M., Kendrick, K. M., Zhang, J., Luo, Q., Liu, Z., Yu, R., Deng, W., Wang, Q., Ma, X., Guo, W., Francis, S., Liddle, P., Mayer, A. R., Schumann, G., Li, T., Feng, J., May 2015. Voxel-based, brain-wide association study of aberrant functional connectivity in schizophrenia implicates thalamocortical circuitry. Npj Schizophrenia 1, –.
URL http://dx.doi.org/10.1038/npjschz.2015.16

Cho, Z. H., Chung, S. C., Lim, D. W., Wong, E. K., Feb 1998. Effects of the acoustic noise of the gradient systems on fmri: a study on auditory, motor, and visual cortices. Magn Reson Med 39 (2), 331–335.

Collins, D. L., Zijdenbos, A. P., Kollokian, V., Sled, J. G., Kabani, N. J., Holmes, C. J., Evans, A. C., Jun. 1998. Design and construction of a realistic digital brain phantom. IEEE Trans Med Imaging 17 (3), 463–468.
URL http://view.ncbi.nlm.nih.gov/pubmed/9735909

Cullen, K. R., Gee, D. G., Klimes-Dougan, B., Gabbay, V., Hulvershorn, L., Mueller, B. A., Camchong, J., Bell, C. J., Houri, A., Kumra, S., Lim, K. O., Castellanos, F. X., Milham, M. P., Sep 2009. A preliminary study of functional connectivity in comorbid adolescent depression. Neurosci Lett 460 (3), 227–231.
URL http://dx.doi.org/10.1016/j.neulet.2009.05.022

Damoiseaux, J. S., Prater, K. E., Miller, B. L., Greicius, M. D., Apr. 2012. Functional connectivity tracks clinical deterioration in Alzheimer's disease. Neurobiology of Aging 33 (4), 828.e19–828.e30.
URL http://dx.doi.org/10.1016/j.neurobiolaging.2011.06.024

Damoiseaux, J. S., Rombouts, S. A. R. B., Barkhof, F., Scheltens, P., Stam, C. J., Smith, S. M., Beckmann, C. F., Sep. 2006. Consistent resting-state networks across healthy subjects. Proceedings of the National Academy of Sciences 103 (37), 13848–13853.
URL http://dx.doi.org/10.1073/pnas.0601417103

Dansereau, C., Orban, P., Bellec, P., 2014. Impact of motion on resting-state fmri connectivity in healthy aging and alzheimer's disease, and possible remedies. Vol. 10. pp. P49 –, alzheimer's Association International Conference 2014 Alzheimer's Association International Conference 2014.
URL http://www.sciencedirect.com/science/article/pii/S1552526014007389

Dansereau, C., Risterucci, C., Pich, E. M., Arnold, D., Bellec, P., 2013. A power analysis for multisite studies in resting-state functional connectivity, with an application to clinical trials in alzheimer's disease. Vol. 9. pp. P248 – P249, alzheimer's Association International Conference 2013 Alzheimer's Association International Conference 2013.
URL http://www.sciencedirect.com/science/article/pii/S1552526013011461

De Luca, M., Beckmann, C. F., De Stefano, N., Matthews, P. M., Smith, S. M., Feb. 2006. fMRI resting state networks define distinct modes of long-distance interactions in the human brain. NeuroImage 29 (4), 1359–1367.
URL http://dx.doi.org/10.1016/j.neuroimage.2005.08.035

Desmond, J., Glover, G., Aug. 2002. Estimating sample size in functional mri (fmri) neuroimaging studies: Statistical power analyses. Journal of Neuroscience Methods 118 (2), 115–128.
URL http://dx.doi.org/10.1016/s0165-0270(02)00121-8

Edward, V., Windischberger, C., Cunnington, R., Erdler, M., Lanzenberger, R., Mayer, D., Endl, W., Beisteiner, R., Nov 2000. Quantification of fmri artifact reduction by a novel plaster cast head holder. Hum Brain Mapp 11 (3), 207–213.

Elliott, M. R., Bowtell, R. W., Morris, P. G., Jun 1999. The effect of scanner sound in visual, motor, and auditory functional mri. Magn Reson Med 41 (6), 1230–1235.

Fair, D. A., Nigg, J. T., Iyer, S., Bathula, D., Mills, K. L., Dosenbach, N. U. F., Schlaggar, B. L., Mennes, M., Gutman, D., Bangaru, S., Buitelaar, J. K., Dickstein, D. P., Martino, A. D., Kennedy, D. N., Kelly, C., Luna, B., Schweitzer, J. B., Velanova, K., Wang, Y.-F., Mostofsky, S., Castellanos, F. X., Milham, M. P., 2012. Distinct neural signatures detected for adhd subtypes after controlling for micro-movements in resting state functional connectivity mri data. Front Syst Neurosci 6, 80.
URL http://dx.doi.org/10.3389/fnsys.2012.00080

Fang, F., Murray, S. O., He, S., Jun 2007. Duration-dependent fmri adaptation and distributed viewer-centered face representation in human visual cortex. Cereb Cortex 17 (6), 1402–1411.
URL http://dx.doi.org/10.1093/cercor/bhl053

Feinberg, D. A., Moeller, S., Smith, S. M., Auerbach, E., Ramanna, S., Gunther, M., Glasser, M. F., Miller, K. L., Ugurbil, K., Yacoub, E., 2010. Multiplexed echo planar imaging for sub-second whole brain fmri and fast diffusion imaging. PLoS One 5 (12), e15710.
URL http://dx.doi.org/10.1371/journal.pone.0015710

Fonov, V., Evans, A. C., Botteron, K., Almli, C. R., McKinstry, R. C., Collins, D. L., Brain Development Cooperative Group, Jan. 2011. Unbiased average age-appropriate atlases for pediatric studies. NeuroImage 54 (1), 313–327.
URL http://dx.doi.org/10.1016/j.neuroimage.2010.07.033

Fox, M. D., Zhang, D., Snyder, A. Z., Raichle, M. E., Jun 2009. The global signal and observed anticorrelated resting state brain networks. J Neurophysiol 101 (6), 3270–3283.
URL http://dx.doi.org/10.1152/jn.90777.2008

Friedman, L., Glover, G., Jun. 2006. Report on a multicenter fmri quality assurance protocol. Journal of magnetic resonance imaging : JMRI 23 (6), 827–839.
URL http://dx.doi.org/10.1002/jmri.20583

Friedman, L., Glover, G., Consortium, T. F., Nov. 2006. Reducing interscanner variability of activation in a multicenter fmri study: Controlling for signal-to-fluctuation-noise-ratio (sfnr) differences. NeuroImage 33 (2), 471–481.
URL http://dx.doi.org/10.1016/j.neuroimage.2006.07.012

Giove, F., Gili, T., Iacovella, V., Macaluso, E., Maraviglia, B., Oct. 2009. Images-based suppression of unwanted global signals in resting-state functional connectivity studies. Magnetic resonance imaging 27 (8), 1058–1064.
URL http://dx.doi.org/10.1016/j.mri.2009.06.004

Goveas, J. S., Xie, C., Ward, B. D., Wu, Z., Li, W., Franczak, M., Jones, J. L., Antuono, P. G., Li, S.-J. J., Oct. 2011. Recovery of hippocampal network connectivity correlates with cognitive improvement in mild Alzheimer's disease patients treated with donepezil assessed by resting-state fMRI. Journal of magnetic resonance imaging : JMRI 34 (4), 764–773.
URL http://dx.doi.org/10.1002/jmri.22662

Hartstra, E., Khn, S., Verguts, T., Brass, M., Nov 2011. The implementation of verbal instructions: an fmri study. Hum Brain Mapp 32 (11), 1811–1824.
URL http://dx.doi.org/10.1002/hbm.21152

He, Y., Chen, Z., Gong, G., Evans, A., Aug. 2009. Neuronal networks in Alzheimer's disease. The Neuroscientist : a review journal bringing neurobiology, neurology and psychiatry 15 (4), 333–350.
URL http://dx.doi.org/10.1177/1073858409334423

Jafri, M. J. J., Pearlson, G. D. D., Stevens, M., Calhoun, V. D. D., Nov. 2007. A method for functional network connectivity among spatially independent resting-state components in schizophrenia. Neuroimage.
URL http://dx.doi.org/10.1016/j.neuroimage.2007.11.001

Klarhofer, M., Barth, M., Moser, E., May 2002. Comparison of multi-echo spiral and echo planar imaging in functional mri. Magn Reson Imaging 20 (4), 359–364.

Lin, F.-H., Huang, T.-Y., Chen, N.-K., Wang, F.-N., Stufflebeam, S. M., Belliveau, J. W., Wald, L. L., Kwong, K. K., Aug 2005. Functional mri using regularized parallel imaging acquisition. Magn Reson Med 54 (2), 343–353.
URL http://dx.doi.org/10.1002/mrm.20555

Lu, Y., Jiang, T., Zang, Y., Sep. 2003. Region growing method for the analysis of functional MRI data. NeuroImage 20 (1), 455–465.
URL http://dx.doi.org/10.1016/S1053-8119(03)00352-5

Lund, T. E., Madsen, K. H., Sidaros, K., Luo, W.-L., Nichols, T. E., Jan. 2006. Non-white noise in fMRI: does modelling have an impact? NeuroImage 29 (1), 54–66.
URL http://dx.doi.org/10.1016/j.neuroimage.2005.07.005

Marrelec, G., Bellec, P., Krainik, A., Duffau, H., Pélégrini-Issac, M., Lehéricy, S., Benali, H., Doyon, J., Feb. 2008. Regions, systems, and the brain: Hierarchical measures of functional integration in fMRI. Medical image analysis.
URL http://dx.doi.org/10.1016/j.media.2008.02.002

Menon, V., Lim, K., Anderson, J., Johnson, J., Pfefferbaum, A., 1997. Design and efficacy of a head-coil bite bar for reducing movement-related artifacts during functional mri scanning. Behavior Research Methods, Instruments, & Computers 29 (4), 589–594.
URL http://dx.doi.org/10.3758/BF03210613

Mueller, S. G., Weiner, M. W., Thal, L. J., Petersen, R. C., Jack, C., Jagust, W., Trojanowski, J. Q., Toga, A. W., Beckett, L., Nov 2005. The alzheimer's disease neuroimaging initiative. Neuroimaging Clin N Am 15 (4), 869–77, xi–xii.
URL http://dx.doi.org/10.1016/j.nic.2005.09.008

Murphy, K., Birn, R. M., Handwerker, D. A., Jones, T. B., Bandettini, P. A., Feb. 2009. The impact of global signal regression on resting state correlations: are anti-correlated networks introduced? NeuroImage 44 (3), 893–905.
URL http://dx.doi.org/10.1016/j.neuroimage.2008.09.036

Nielsen, J., Zielinski, B., Fletcher, T., Alexander, A., Lange, N., Bigler, E., Lainhart, J., Anderson, J., 2013. Multisite functional connectivity mri classification of autism: Abide results. Frontiers in human neuroscience 7, –.
URL http://view.ncbi.nlm.nih.gov/pubmed/24093016

Power, J. D., Barnes, K. A., Snyder, A. Z., Schlaggar, B. L., Petersen, S. E., Feb. 2012. Spurious but systematic correlations in functional connectivity MRI networks arise from subject motion. NeuroImage 59 (3), 2142–2154.
URL http://dx.doi.org/10.1016/j.neuroimage.2011.10.018

Power, J. D., Mitra, A., Laumann, T. O., Snyder, A. Z., Schlaggar, B. L., Petersen, S. E., Jan. 2014. Methods to detect, characterize, and remove motion artifact in resting state fMRI. NeuroImage 84, 320–341.
URL http://dx.doi.org/10.1016/j.neuroimage.2013.08.048

Rorden, C., Karnath, H.-O., Bonilha, L., Jul 2007. Improving lesion-symptom mapping. J Cogn Neurosci 19 (7), 1081–1088.
URL http://dx.doi.org/10.1162/jocn.2007.19.7.1081

Saad, Z. S., Gotts, S. J., Murphy, K., Chen, G., Jo, H. J. J., Martin, A., Cox, R. W., 2012. Trouble at rest: how correlation patterns and group differences become distorted after global signal regression. Brain connectivity 2 (1), 25–32.
URL http://dx.doi.org/10.1089/brain.2012.0080

Shehzad, Z., Kelly, C. M., Reiss, P. T., Gee, D. G., Gotimer, K., Uddin, L. Q., Lee, S. H. H., Margulies, D. S., Roy, A. K. K., Biswal, B. B., Petkova, E., Castellanos, F. X., Milham, M. P., Oct. 2009. The resting brain: unconstrained yet reliable. Cerebral cortex (New York, N.Y. : 1991) 19 (10), 2209–2229.
URL http://dx.doi.org/10.1093/cercor/bhn256

Thirion, B., Dodel, S., Poline, J. B., Jan. 2006. Detection of signal synchronizations in resting-state fMRI datasets. Neuroimage 29 (1), 321–327.
URL http://dx.doi.org/10.1016/j.neuroimage.2005.06.054

Tomasi, D., Volkow, N. D., May 2010. Functional connectivity density mapping. Proceedings of the National Academy of Sciences 107 (21), 9885–9890.
URL http://dx.doi.org/10.1073/pnas.1001414107

Tzourio-Mazoyer, N., Landeau, B., Papathanassiou, D., Crivello, F., Etard, O., Delcroix, N., Mazoyer, B., Joliot, M., Jan. 2002. Automated anatomical labeling of activations in SPM using a macroscopic anatomical parcellation of the MNI MRI single-subject brain. NeuroImage 15 (1), 273–289.
URL http://dx.doi.org/10.1006/nimg.2001.0978

Van Dijk, K. R., Hedden, T., Venkataraman, A., Evans, K. C., Lazar, S. W., Buckner, R. L., Jan. 2010. Intrinsic functional connectivity as a tool for human connectomics: theory, properties, and optimization. Journal of neurophysiology 103 (1), 297–321.
URL http://dx.doi.org/10.1152/jn.00783.2009

Vanhoutte, G., Verhoye, M., der Linden, A. V., May 2006. Changing body temperature affects the t2* signal in the rat brain and reveals hypothalamic activity. Magn Reson Med 55 (5), 1006–1012.
URL http://dx.doi.org/10.1002/mrm.20861

Wang, K., Liang, M., Wang, L., Tian, L., Zhang, X., Li, K., Jiang, T., Oct. 2007. Altered functional connectivity in early Alzheimer's disease: a resting-state fMRI study. Human brain mapping 28 (10), 967–978.
URL http://dx.doi.org/10.1002/hbm.20324

Wang, L., Zang, Y., He, Y., Liang, M., Zhang, X., Tian, L., Wu, T., Jiang, T., Li, K., Jun. 2006. Changes in hippocampal connectivity in the early stages of Alzheimer's disease: evidence from resting state fMRI. NeuroImage 31 (2), 496–504.
URL http://dx.doi.org/10.1016/j.neuroimage.2005.12.033

Yan, C., Liu, D., He, Y., Zou, Q., Zhu, C., Zuo, X., Long, X., Zang, Y., May 2009. Spontaneous Brain Activity in the Default Mode Network Is Sensitive to Different Resting-State Conditions with Limited Cognitive Load. PLoS ONE 4 (5), e5743+.
URL http://dx.doi.org/10.1371/journal.pone.0005743

Yan, C.-G., Cheung, B., Kelly, C., Colcombe, S., Craddock, R. C., Di Martino, A., Li, Q., Zuo, X.-N., Castellanos, F. X., Milham, M. P., Aug. 2013a. A comprehensive assessment of regional variation in the impact of head micromovements on functional connectomics. NeuroImage 76, 183–201.
URL http://dx.doi.org/10.1016/j.neuroimage.2013.03.004

Yan, C.-G. G., Craddock, C. C., Zuo, X.-N. N., Zang, Y.-F. F., Milham, M. P., Oct. 2013b. Standardizing the intrinsic brain: towards robust measurement of inter-individual variation in 1000 functional connectomes. NeuroImage 80, 246–262.
URL http://view.ncbi.nlm.nih.gov/pubmed/23631983

Yang, H., Long, X.-Y., Yang, Y., Yan, H., Zhu, C.-Z., Zhou, X.-P., Zang, Y.-F., Gong, Q.-Y., May 2007. Amplitude of low frequency fluctuation within visual areas revealed by resting-state functional mri. Neuroimage 36 (1), 144–152.
URL http://dx.doi.org/10.1016/j.neuroimage.2007.01.054

Zhang, H., Wang, S., Xing, J., Liu, B., Ma, Z., Yang, M., Zhang, Z., Teng, G., Jan. 2009. Detection of PCC functional connectivity characteristics in resting-state fMRI in mild Alzheimer's disease. Behavioural Brain Research 197 (1), 103–108.
URL http://dx.doi.org/10.1016/j.bbr.2008.08.012

Zhang, H., Zuo, X.-N., Ma, S.-Y., Zang, Y.-F., Milham, M. P., Zhu, C.-Z., Mar. 2010. Subject Order-Independent Group ICA (SOI-GICA) for Functional MRI Data Analysis. NeuroImage.
URL http://dx.doi.org/10.1016/j.neuroimage.2010.03.039

Zijdenbos, A. P., Forghani, R., Evans, A. C., Oct. 2002. Automatic "pipeline" analysis of 3-D MRI data for clinical trials: application to multiple sclerosis. IEEE Transactions on Medical Imaging 21 (10), 1280–1291.
URL http://dx.doi.org/10.1109/TMI.2002.806283

Zuo, X.-N., Xu, T., Jiang, L., Yang, Z., Cao, X.-Y., He, Y., Zang, Y.-F., Castellanos, F. X., Milham, M. P., Oct. 2012. Toward reliable characterization of functional homogeneity in the human brain: Preprocessing, scan duration, imaging resolution and computational space. NeuroImage.
URL http://dx.doi.org/10.1016/j.neuroimage.2012.10.017

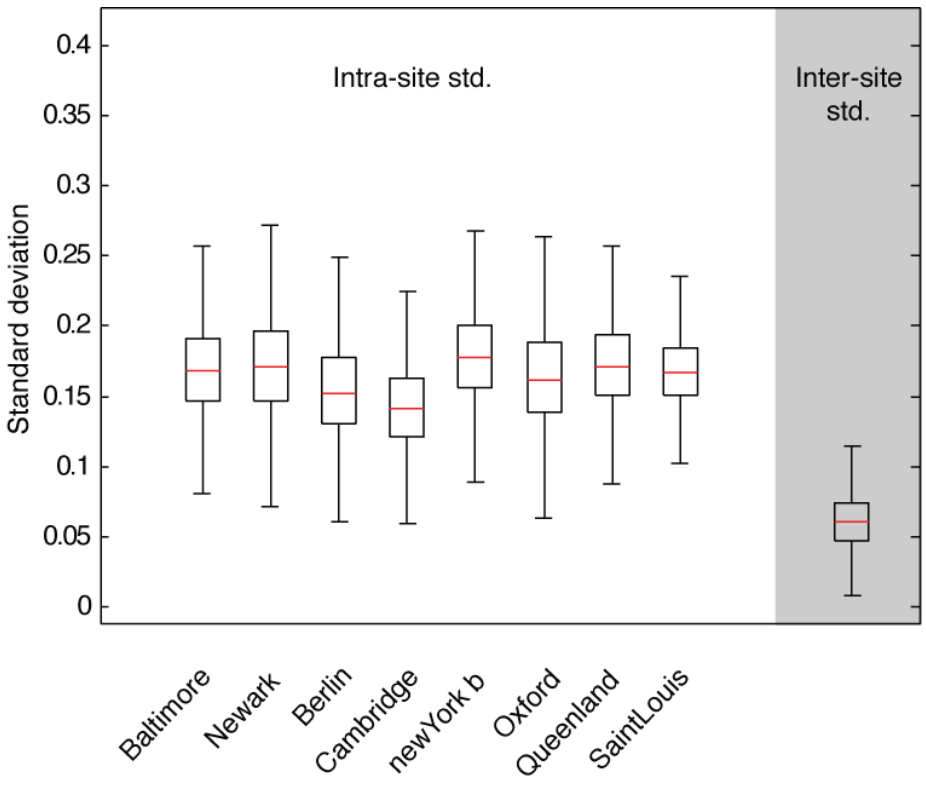

Figure 1: Distribution of intra-site (between-subject) standard deviation vs. inter-site (between-site) standard deviation, based on the standard deviation of the connectivity matrices from 8 sites from the 1000 functional connectome dataset.

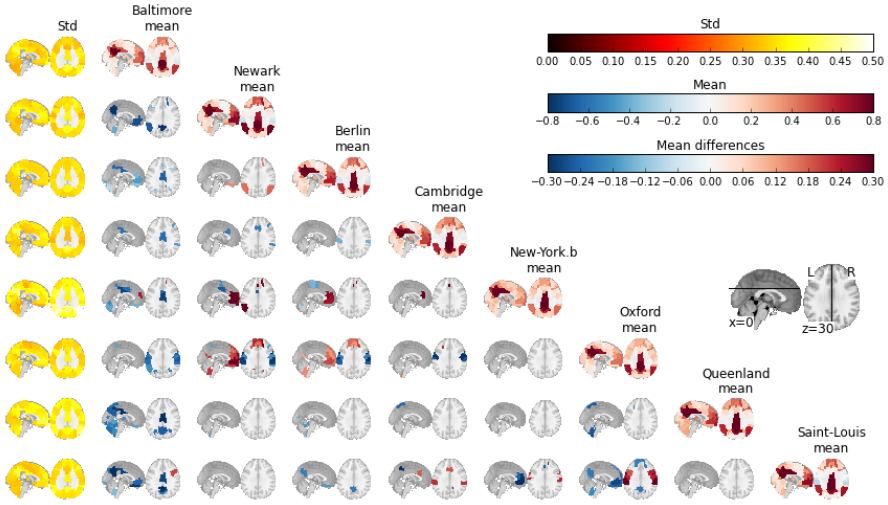

Figure 2: Functional connectivity maps of the default-mode network at multiple sites. The average connectivity map are shown on the diagonal (left). The standard deviation across subjects and within site is shown on the first column. Each off-diagonal block represent the significant differences between the average functional connectivity maps between two sites (called the inter-site bias).

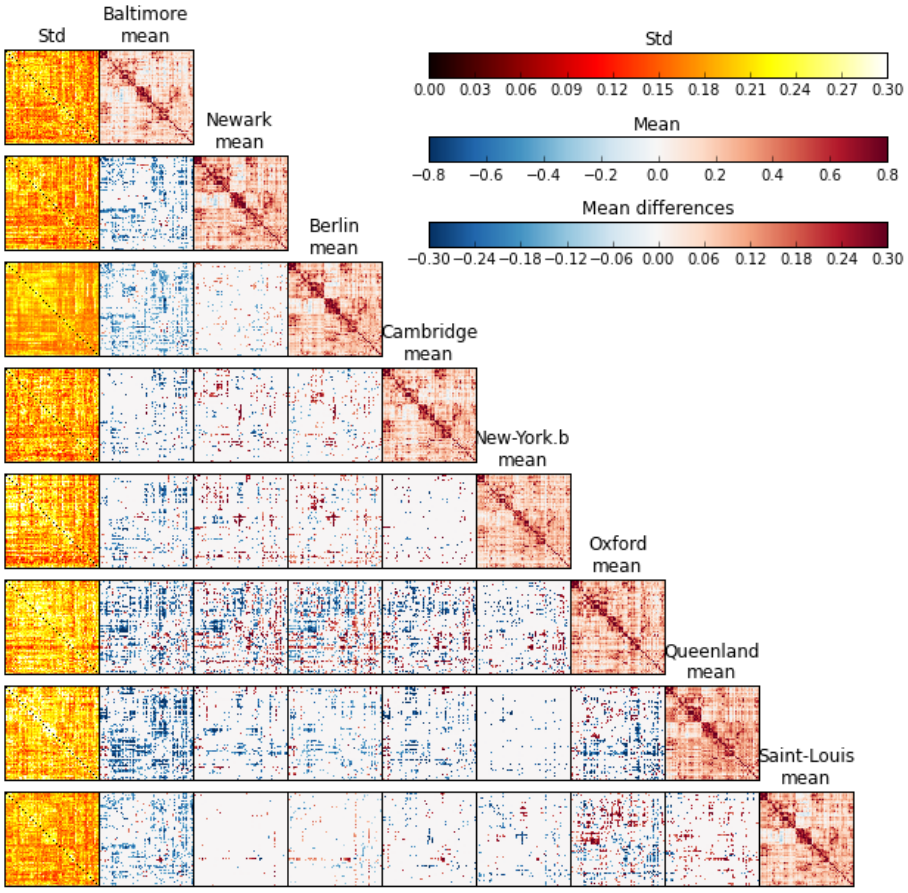

Figure 3: Functional connectome for multiple sites. The average connectome of 8 sites (Baltimore, Newark, Berlin, Cambridge, New-Yorkb, Oxford, Queenland and SaintLouis at 3T) are shown on the diagonal (left). The standard deviation across subjects and within site is shown on the first column. Each off-diagonal block represent the absolute difference between the average functional connectivity maps between two sites (called the inter-site bias).

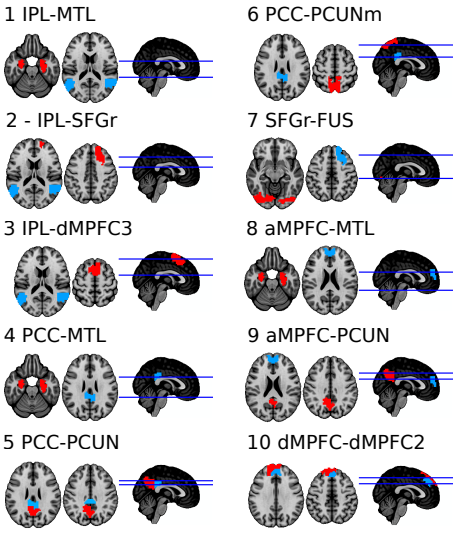

Connexions pair based on a literature review

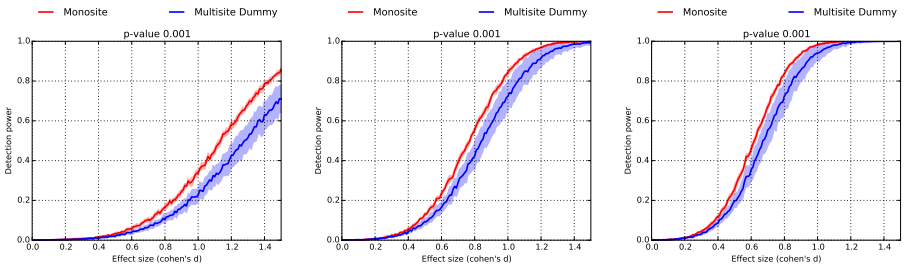

40 subjects 80 subjects 120 subjects

Simulation on real data, detection power of two groups balanced 50%-50% between 7 sites. Two scenarios, 1) monosite and 2) multisite 7 sites with correction for multisite differences using dummy variables. Each plot show the detection power in function of the effect size for 3 different sample size 40, 80 and 120 subjects in total.

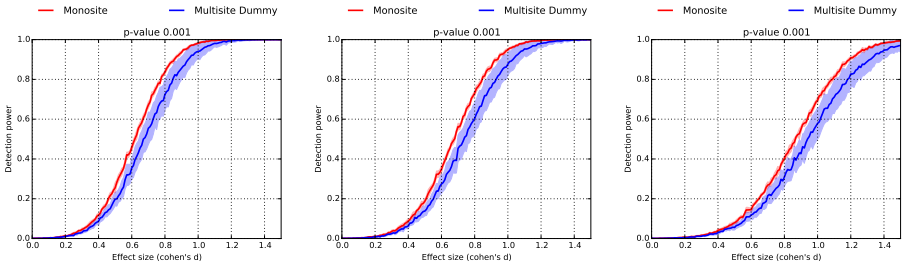

Debalancing 50% Debalancing 30% Debalancing 15%

Simulation on real data, detection power of two groups for a total of 120 subject between 7 sites. All plot show two scenarios, 1) monosite and 2) multisite 7 sites with correction for multisite differences using dummy variables.

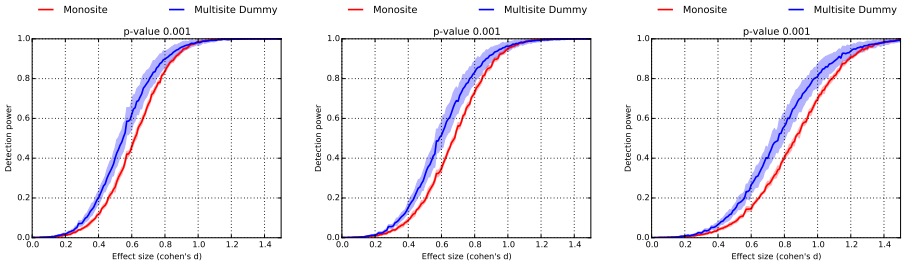

Debalancing 50% Debalancing 30% Debalancing 15%

Simulation on real data, detection power of two groups for a total of 120 subject between 7 sites. All plot show two scenarios, 1) monosite and 2) multisite 7 sites with correction for multisite differences using dummy variables.

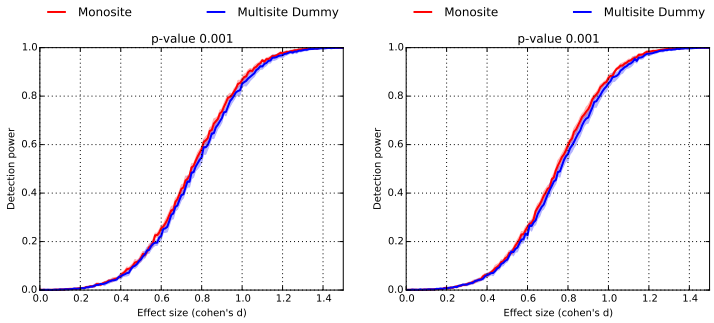

30%-70% 70%-30%

Simulation on real data, detection power of two groups for a total of 100 subject between 2 sites, one small site of 20 subjects and one large of 80 subjects. All plot show two scenarios, 1) monosite and 2) multisite 2 sites with correction for multisite differences using dummy variables. Simulation of the detection power of two groups balanced 30% and 70% between 2 sites.

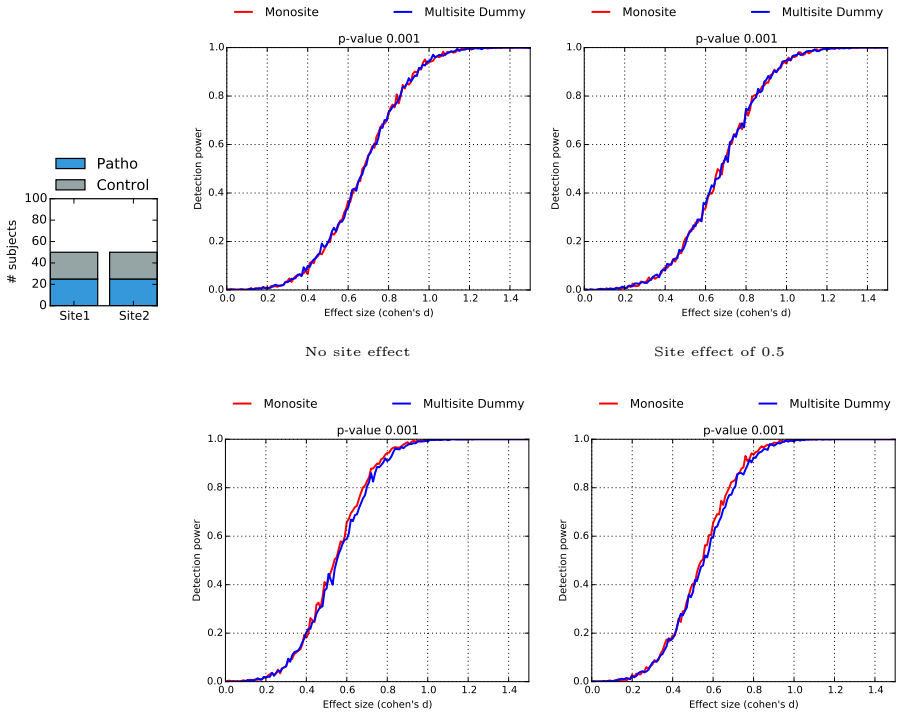

Simulation of the detection power of two groups balanced 50%-50% between two sites. All plots show four scenarios in two configuration one monosite and two sites with correction for multisite differences using dummy variables. The first column represent scenarios without site effect and the second column show with a site effect the first row show simulation with out interaction site-pathology and the second row show with interaction.

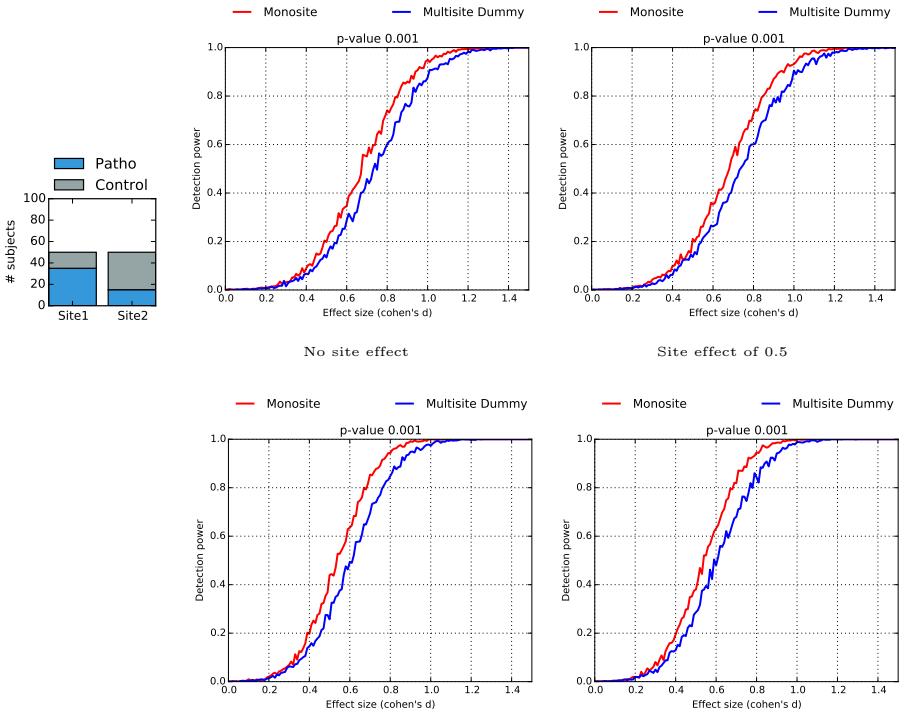

Simulation of the detection power of two groups unbalanced 70%-30% between two sites. All plots show four scenarios in two configuration one monosite and two sites with correction for multisite differences using dummy variables. The first column represent scenarios without site effect and the second column show with a site effect the first row show simulation with out interaction site-pathology and the second row show with interaction.

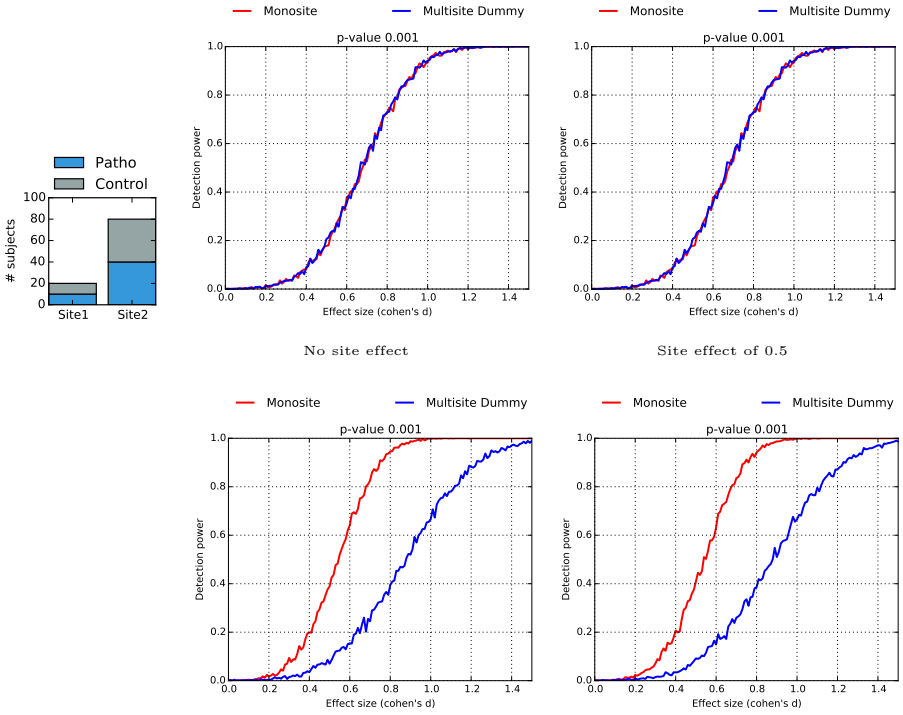

Simulation of the detection power of two groups unbalanced 50%-50% between two sites, one small site of 20 subjects and one large of 80 subjects. All plots show four scenarios in two configuration one monosite and two sites with correction for multisite differences using dummy variables. The first column represent scenarios without site effect and the second column show with a site effect the first row show simulation with out interaction site-pathology and the second row show with interaction.

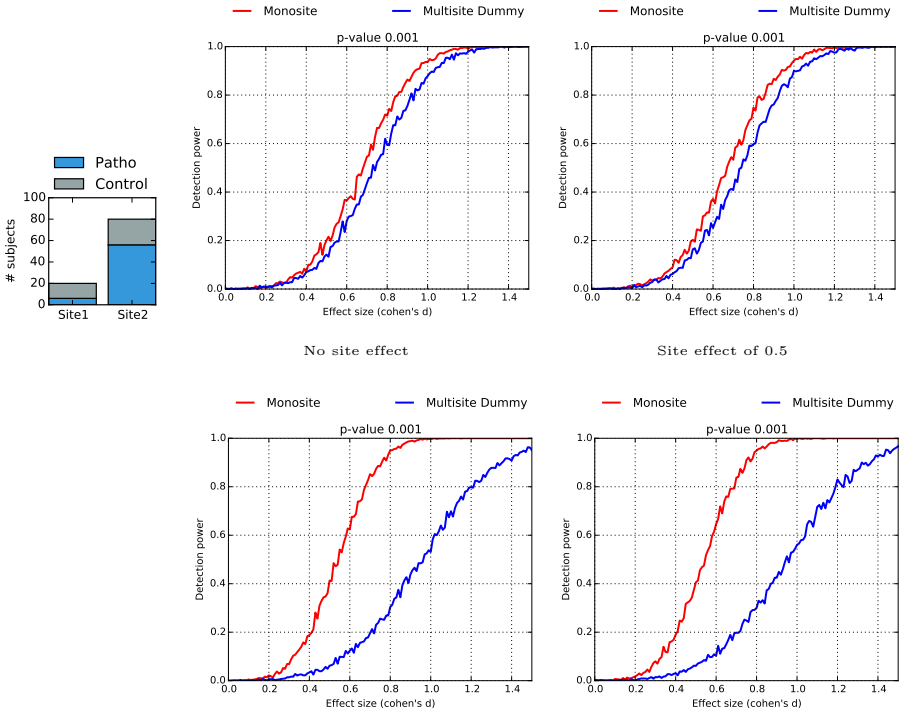

Simulation of the detection power of two groups unbalanced 70%-30% between two sites, one small site of 20 subjects and one large of 80 subjects. All plots show four scenarios in two configuration one monosite and two sites with correction for multisite differences using dummy variables. The first column represent scenarios without site effect and the second column show with a site effect the first row show simulation with out interaction site-pathology and the second row show with interaction.

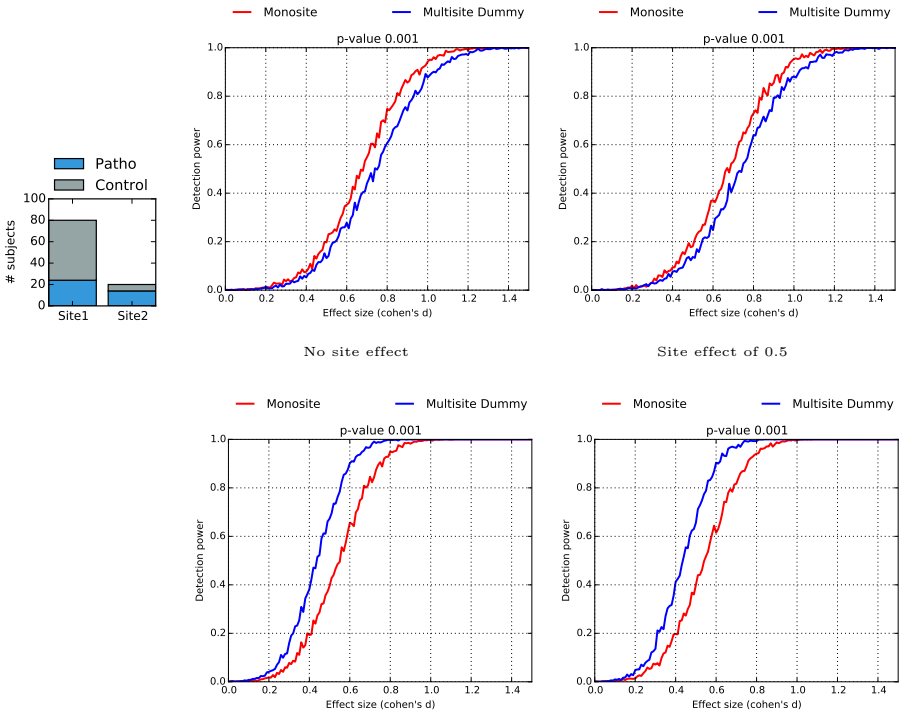

No site effect | Site effect of 0.5

Interac site-patho, no site effect | Interac site-patho + site effect

Simulation of the detection power of two groups unbalanced 70%-30% between two sites, one small site of 20 subjects and one large of 80 subjects. All plots show four scenarios in two configuration one monosite and two sites with correction for multisite differences using dummy variables. The first column represent scenarios without site effect and the second column show with a site effect the first row show simulation with out interaction site-pathology and the second row show with interaction.

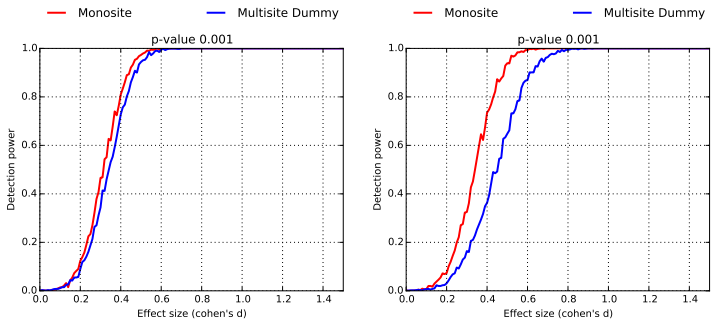

No interaction site-patho | Site effect of 0.5

Simulation of the detection power of two groups balanced randomly between 10%-90% between 50 sites, the number of subject per site is randomly assigned between 2 and 15. All plot show four scenario, one monosite and two sites with correction for multisite differences using dummy variables. The plots show the detection power when the variability is greater in one side then the other for the pathology group (twice the reference variability in one site and half the reference variability in the other one)

Supplementary Material – Feasibility of multi-centric fMRI connectivity studies of Alzheimer's disease

Submitted to Neuroimage.

C. Dansereau[1,2], C. Risterucci[3], E. Merlo Pich[3], D. Arnold[4], P. Bellec[1,2]

[1]Functional Neuroimaging Unit, Centre de Recherche de l'Institut Universitaire de Gériatrie de Montréal
[2]Department of Computer Science and Operations Research, University of Montreal, Montreal, Quebec, Canada
[3]F. Hoffmann-La Roche Ldt., Basel, Switzerland
[4]NeuroRx, Montreal, Quebec, Canada

For all questions regarding the paper, please address correspondence to Pierre Bellec, CRIUGM, 4545 Queen Mary, Montreal, QC, H3W 1W5, Canada. Email: pierre.bellec (at) criugm.qc.ca.

Literature review: Alzheimers disease and resting-state fMRI

- Zhang et al. (2009) used functional connectivity maps with a seed in the posterior cingulate cortex (PCC) to explore the differences between a group of elderly cognitively normal subjects (CNE, n=16) and patients with a mild dementia of the Alzheimers type (DAT, n=18).

- Zhang et al. (2010) generalized the Zhang et al. (2009) study with CNE (n=16) and a larger group of patients with DAT (n=46). Patients were separated in three groups (mild, moderate, severe DAT), and each group of patients was contrasted against the CNE.

- Wang et al. (2006) used functional connectivity maps with a seed in the hippocampi to explore the differences between a group of CNE (n=13) and patients with a mild DAT (n=13). All results included in the meta-analysis are from Table 2, seeded in the right hippocampus. Seeds were manually delineated on an individual basis.

- Wang et al. (2007) used functional connectivity maps with a seed in the posterior cingulate cortex (PCC) as well as full brain point-to-point correlations (based on an AAL parcellation) to explore the differences between a group of elderly cognitively normal subjects (CNE, n=14) and patients with a very mild to mild dementia of the Alzheimers type (DAT, n=14). Only the results based on the PCC seed were included in the meta-analysis.

- Goveas et al. (2011) used functional connectivity maps with a seed in the hippocampi to explore the differences between a group of elderly cognitively normal subjects (CNE, n=18) and patients with a mild dementia of

the Alzheimers type (DAT, n=14) before and after donepezil treatment. Seeds were manually delineated on an individual basis, before and after treatment.

- Damoiseaux et al. (2012) used dual-regression independent component analysis to explore longitudinal differences between a group of CNE (n=18) and patients with DAT (n=21). All results included in the meta-analysis are from Table 3 (differences at baseline) and Table 4 (interaction with time). The authors used three components representing the Anterior DMN, Ventral DMN and Posterior DMN.